*Weed Science*

**www.cambridge.org/wsc**

# Integrating machine learning and path planning for UAS-based weed recognition and site-specific management in turfgrass systems

Bholuram Gurjar[1,2], Ubaldo Torres[1], Robert Hardin[3], Chase Straw[4,5] and Muthukumar Bagavathiannan[6]

[1]Graduate Research Assistant, Department of Soil and Crop Sciences, Texas A&M University, College Station, TX, USA; [2]Graduate Student, Department of Biological and Agricultural Engineering, Texas A&M University, College Station, TX, USA; [3]Associate Professor, Department of Biological and Agricultural Engineering, Texas A&M University, College Station, TX, USA; [4]Assistant professor, Department of Soil and Crop Sciences, Texas A&M University, College Station, TX, USA; [5]Department of Plant Science, Pennsylvania State University, University Park, PA, USA and [6]Billie Turner Professor of Agronomy, Department of Soil and Crop Sciences, Texas A&M University, College Station, TX, USA

## Research Article

**Cite this article:** Gurjar B, Torres U, Hardin R, Straw C, Bagavathiannan M (2026). Integrating machine learning and path planning for UAS-based weed recognition and site-specific management in turfgrass systems. Weed Sci. **74**(e61), 1–12. doi: 10.1017/wsc.2026.10104

Received: 29 October 2025
Revised: 12 February 2026
Accepted: 5 March 2026

**Associate Editor:**
Jialin Yu, Peking University Institute of Advanced Agricultural Sciences

**Keywords:**
AI/ML; annual bluegrass; drone; neural networks; *Poa*; precision turfgrass management; site-specific weed management; UAV; YOLO

**Corresponding author:**
Muthukumar Bagavathiannan;
Email: muthu.bagavathiannan@tamu.edu

## Abstract

Annual bluegrass (*Poa annua* L.) is an extremely problematic weed in turfgrass, posing a significant challenge for turfgrass management. Injudicious use of herbicides for controlling this weed has led to resistance issues and environmental concerns. Site-specific weed control offers an opportunity to achieve effective weed control with less herbicide use, but it requires the development of a pipeline for weed detection and localization, as well as a path planning algorithm (PPA). To achieve this, unmanned aerial system (UAS)-based RGB imagery of *P. annua* plants in bermudagrass [*Cynodon dactylon* (L.) Pers.] turf was collected at different weed growth stages at two locations in Texas: Deer Park and College Station. A convolutional neural network (CNN) You Only Look Once (YOLO11) and a real-time detection transformer (RT-DETR) model were evaluated for weed detection. The results showed that the YOLO11n model achieved the highest F1 score (0.64) and mean average precision (mAP)@0.50 (0.68), while the RT-DETR-x model achieved the lowest F1 score (0.52) and mAP@0.50 (0.51). The GeoTransform function transforms image coordinates into a world coordinate system with centimeter-level accuracy (mean error = 1.5 cm). However, the precision of the transformation depends on the quality of the orthophoto georeferencing. Additionally, the PPA showed a significant reduction (37.7%) in travel distance compared with the original weed model–derived distance. The research highlighted the potential of UAS-based imagery for weed detection and localization in turfgrass. Further improvements are needed to enhance model performance by modifying the model architecture (e.g., input image size, hyperparameters) and evaluating its robustness across different weed growth stages and turfgrass species.

## Introduction

Effective weed detection and localization are crucial for site-specific weed control (SSWC) in commercial turfgrass systems, such as athletic complexes, golf courses, and sod farms. These systems typically encompass large, intensively managed areas where uniform herbicide applications and mechanical removal are costly, labor-intensive, and increasingly constrained by environmental regulations. SSWC facilitates optimal resource allocation, early intervention, and customized control strategies, fostering data-driven decision-making in turfgrass management (Westwood et al. 2018). Weed detection is the primary step in SSWC, requiring accurate identification of weed plants for tailored control treatments (Tu et al. 2001). Differences in weed morphology and physiology among the species necessitate distinct herbicide management strategies (Beckie 2006). Mowing is a popular weed management strategy in turfgrass, but it is only effective on upright-growing species (e.g., Canada thistle *[Cirsium arvense* (L.) Scop] and dallisgrass [*Paspalum dilatatum* Poir.]), and generally less effective on prostrate or low-growing weeds such as prostrate knotweed (*Polygonum aviculare* L.) and white clover (*Trifolium repens* L.) (Busey 2003; DeBels et al. 2012). Thus, identifying the specific species, growth stage, and characteristics can help effectively implement SSWC. Moreover, accurate weed plant localization reduces off-target application and resource wastage (Esposito et al. 2021; Swinton 2005).

Computer vision (CV) and machine learning (ML) technologies are increasingly important for developing weed detection capabilities that enable SSWC in agriculture. Coleman et al. (2022) reviewed 50 yr of research on weed detection, highlighting the potential utility of deep learning (DL) models for SSWC. The CV and DL technologies enable the development of automated weed

© The Author(s), 2026. Published by Cambridge University Press on behalf of Weed Science Society of America. This is an Open Access article, distributed under the terms of the Creative Commons Attribution licence (https://creativecommons.org/licenses/by/4.0/), which permits unrestricted re-use, distribution and reproduction, provided the original article is properly cited.

Downloaded from https://www.cambridge.org/core. UNIVERSIDAD AUTONOMA METROPOLITANA, on 16 Nov 2026 at 20:06:17, subject to the Cambridge Core terms of use, available at https://www.cambridge.org/core/terms. https://doi.org/10.1017/wsc.2026.10104

recognition systems, significantly reducing labor costs and agricultural inputs (Rai et al. 2023). Researchers have investigated weed detection in turfgrass using deep convolutional neural network (CNN) models and other image processing techniques. For instance, Yu et al. (2019a, 2019b) have identified multiple weed species, including dandelion (*Taraxacum officinale* F.H. Wigg.), ground ivy (*Glechoma hederacea* L.), spotted spurge [*Chamaesyce maculata* (L.) Small; syn.: *Euphorbia maculata* L.], dollar weed (*Hydrocotyle* spp.), old world diamond-flower [*Oldenlandia corymbosa* L.; syn.: *Hedyotis corymbosa* (L.) Lam.], and Florida pusley (*Richardia scabra* L.), achieving high classification accuracy (F1 scores > 0.95) within perennial ryegrass (*Lolium perenne* L.) and common bermudagrass [*Cynodon dactylon* (L.) Pers.] turf. The F1 score, a common metric for evaluating DL models, represents the weighted average of precision and recall, with values ranging from 0 to 1, where 0 indicates extremely poor performance of the model (Yacouby and Axman 2020).

Zhang et al. (2021) evaluated the residual neural network (ResNet) architecture for general weed detection in sod fields using unmanned aerial system (UAS) imagery, reporting detection accuracies ranging from 57% to 90%. Similarly, Parra et al. (2020) and Hahn et al. (2021) explored edge detection techniques and random forest models to identify weeds such as *T. repens*, daisy (*Bellis perennis* L.), and yarrow (*Achillea millefolium* L.) in turfgrass. Meanwhile, Xie et al. (2021) developed a probabilistic map-based algorithm for yellow nutsedge (*Cyperus esculentus* L.) detection in turfgrass, achieving promising results by reducing image labeling time by 95%. These collective research efforts underscore the importance of tailored approaches for effective weed detection in diverse turfgrass systems.

The CNN models can be used to detect weeds and locate them within an image, enabling targeted treatments using CV-based smart-sprayers (Jin et al. 2022; Petelewicz et al. 2024). Jin et al. (2023) developed a grid-based spraying system for treating weeds in dormant bermudagrass, but real-time weed detection and treatment remain a challenge in actively growing bermudagrass (Yu et al. 2019b). Additionally, localization based on grid cell values requires applicators to traverse entire fields, which is inefficient when weed populations are heterogeneous. In contrast, Zhang et al. (2020) utilized the You Only Look Once (YOLOv3) model to convert UAS image pixel coordinates into geodetic coordinates, achieving a low average positional error of 0.1 m. This advancement enables precise weed localization, facilitating the use of GPS-equipped UAS and ground sprayers for SSWC (Gerhards and Oebel 2006).

Weeds are often unevenly distributed across fields, making it crucial to optimize the total path length to improve the efficiency of an applicator. For example, the limited battery life of a UAS sprayer (20 to 25 min) restricts its ability to cover a large area (Vijayakumar et al. 2025). However, with optimized path planning, a UAS sprayer can treat weeds over a larger area with the same battery power. Plessen (2025) evaluated the application of the traveling salesman problem for path planning in spot spraying with UAS sprayers, showing promising results in optimizing the total path length. The path planning algorithm (PPA) minimizes redundant flight time by determining the optimal shortest route for the UAS sprayer to cover all designated spray points.

Annual bluegrass (*Poa annua* L.) has developed resistance to multiple herbicide modes of action in turfgrass systems (Breeden et al. 2017; Brosnan et al. 2020a, 2020b; McCurdy et al. 2023; Patton et al. 2019) and is therefore, a significant challenge for turf managers (Neal 2024; Scherner et al. 2017). Herbicide resistance and the inability to control *P. annua* may compromise the efficiency of turfgrass systems, damaging their aesthetic appeal and functionality (Balogh and Anderson 2020). The application of CV/ML for site-specific management of this weed species has the potential to enhance turfgrass management and sustainability.

Research on weed detection in turfgrass systems is limited, with no studies specifically focused on detecting *P. annua*. Detection of small, green *P. annua* in dense, mowed turfgrass, such as bermudagrass, can be particularly challenging. Additionally, it remains unknown whether UAS-based imagery can be used to effectively detect and localize *P. annua* in turfgrass. To develop an effective framework for weed detection and localization in turf, it is imperative to address these knowledge gaps. Therefore, the specific objectives of this study were: (1) to detect *P. annua* in bermudagrass turf using UAS imagery and ML techniques; (2) to localize individual weed plants using ML tools for SSWC; and (3) to optimize path planning for efficient UAS-based targeting of spatially distributed *P. annua* plants.

## Materials and Methods

### Data Collection

Experiments were conducted during the springs of 2023 and 2024 at three locations: the Deer Park Soccer Complex (29.70363889, −95.09997222) in Deer Park, TX, with 'Tifway 419' hybrid bermudagrass; the Scotts Miracle-Gro Facility for Lawn and Garden Research (30.618333, −96.365694) in College Station, TX, with common bermudagrass; and the Simpson Drill Field (30.613833, −96.342611) at Texas A&M University, College Station, TX, with Tifway 419 hybrid bermudagrass. A DJI Phantom 4 Pro (12 MP RGB camera) and a DJI Phantom 4 RTK (20 MP RGB camera, SZ DJI® Technology, Shenzhen, Guangdong, China) UAS were used to collect images of seedling, vegetative, and flowering stages of *P. annua*. Different growth stages (germination to flowering) of *P. annua* were included as part of a diverse image dataset for training the ML models. The UAS images were collected in both manual and autonomous modes under different illumination conditions (e.g., sunny, partially cloudy, and cloudy) and turfgrass environments to create a diverse dataset for developing a robust *P. annua* detection algorithm in bermudagrass (Figure 1). The flight altitude of the manual aerial data collection ranged from 1.5 to <5 m, while the autonomous mode was at 5 m. The autonomous flight mode images were captured in a grid pattern with 70% front and side overlap. To ensure accurate georeferencing, six ground control points (GCPs) were deployed across the field, and a handheld real-time kinematic (RTK) GNSS unit (Emlid Reach2+) was used to collect latitude and longitude coordinates for each GCP.

### Image Annotation and Dataset Preparation

A total of 1,837 UAS images, representing 31,859 instances of *P. annua*, were selected. These images were annotated with bounding boxes using the LabelImg image annotation tool (Tzutalin 2015). The images obtained through both manual and autonomous flight modes were annotated with a single class (labeled as "poa"), and the annotated data were exported in YOLO format. The original UAS imagery, with dimensions of 5,472 (width) by 3,648 (height) pixels, was downscaled to 1,280 by 1,280 pixels to reduce computational requirements, with black padding added to maintain the aspect ratio. To check the dataset's

Downloaded from https://www.cambridge.org/core. UNIVERSIDAD AUTONOMA METROPOLITANA, on 16 Nov 2026 at 20:06:17, subject to the Cambridge Core terms of use, available at https://www.cambridge.org/core/terms. https://doi.org/10.1017/wsc.2026.10104



**Figure 1.** Selected RGB images of *Poa annua* in bermudagrass turf across diverse environmental, management, and growth conditions.

robustness, K-fold cross-validation with K = 5 was used to evaluate the models on the entire dataset (Wong and Yeh 2019).

### Model Selection, Training, and Evaluation

For identifying *P. annua* in bermudagrass turf, two object detection architectures were evaluated: one based on a CNN (YOLO11) (https://github.com/ultralytics/ultralytics) and the other on a transformer (Real-Time Detection Transformer [RT-DETR]) (Zhao et al. 2024). Each model variant was trained with a batch size of four, with six data loader workers, and an input image resolution of 1,280 × 1,280 pixels. The remaining hyperparameters were kept at their default setting during training. The model variants were trained and tested on the Ubuntu 20.04.4 LTS (Canonical Ltd., London, UK) operating system using a 50-GB graphics processing unit (GPU) and a 250-GB random-access memory (RAM). The model's performance was assessed using standard metrics, including precision (P), recall (R), mean average precision (mAP) @0.50, and F1 score (Yacouby and Axman 2020). The experimental units were the individual folds in 5-fold cross-validation for each model variant, and the ANOVA included model variant (i.e., YOLO11, RT-DETR) as the fixed factor. All analyses were performed using JMP® (Pro v. 16.0; SAS Institute Inc., Cary, North Carolina, USA) and treatment mean separations were conducted using Tukey's honestly significant difference (HSD) method, with a significance level of $\alpha = 0.05$.

Downloaded from https://www.cambridge.org/core. UNIVERSIDAD AUTONOMA METROPOLITANA, on 16 Nov 2026 at 20:06:17, subject to the Cambridge Core terms of use, available at https://www.cambridge.org/core/terms. https://doi.org/10.1017/wsc.2026.10104

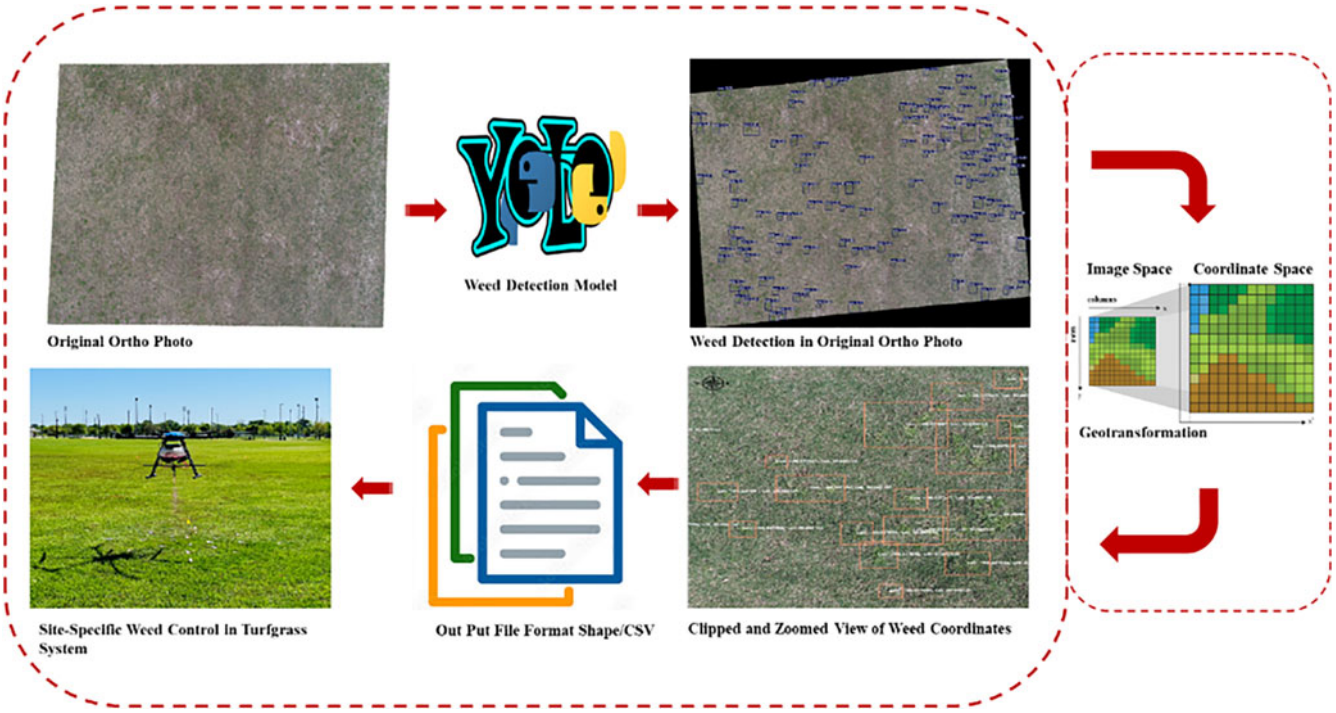



**Figure 2.** A schematic diagram describing the entire workflow, including aerial image collection, analysis, weed map generation, and site-specific control of *Poa annua* in bermudagrass turf.

### Weed Localization

The photogrammetry software Agisoft Metashape v. 1.8.5 (Agisoft®, St Petersburg, Russia) was used to generate orthophotos from images captured in autonomous flight mode (ground sampling distance ≈ 2.8 mm/pixel). These orthophotos were georeferenced, assigning latitude and longitude information to each pixel. A custom-trained ML "poa-weed' model was employed for weed recognition within the orthophotos. Upon weed detection in an image, the center of the bounding box was determined by averaging the $x$ and $y$ coordinates of the top-left ($x_1$, $y_1$) and bottom-right ($x_2$, $y_2$) corners. The GeoTransform function (Anonymous 2025) was then applied to convert the bounding box's center point from image coordinates (pixel, line) to geographic coordinates ($X_{geo}$ = longitude, $Y_{geo}$ = latitude) (Equations 1 and 2).

$$X_geo = GT(0) + X_pixel * GT(1) + Y_line * GT(2) \quad [1]$$

$$Y_geo = GT(3) + X_pixel * GT(4) + Y_line * GT(5) \quad [2]$$

where:

GT(0) is the $x$-coordinate of the upper-left corner of the upper-left pixel,
GT(1) is the pixel resolution/pixel width,
GT(2) is the row rotation,
GT(3) is the $y$-coordinate of the upper-left corner of the upper-left pixel,
GT(4) is the column rotation, and
GT(5) is the pixel resolution/pixel height.

After image coordinates are transformed into geocoordinates, the model output can be in the form of a shapefile or a comma-separated values (CSV) file, depending on user preference; however, both file formats were used in this study (Figure 2). Because the UAS images were captured with a 70% overlap, it is possible for the same weed plant to be detected multiple times in overlapping images, potentially leading to duplicate weed coordinates in the output file. Therefore, a Python script was written to eliminate duplicate coordinates from the input CSV file and generate a new CSV file containing only unique coordinates. However, in the current study, orthophotos were used, and their quality was not affected by the percentage of overlap, allowing for the reduction of overlap in autonomous flight plans. This allows operators to capture larger areas, flying at a low altitude (thus high optical resolution), with the same battery capacity.

### Weed Localization Accuracy Assessment

To verify the accuracy of weed localization, ArcGIS Pro 3.0.0 (ESRI, Redlands, CA, USA) was used. Orthophotos were imported, and the center points of *P. annua* plants were identified and manually marked within each image. To avoid detection errors associated with overlapping images, only the single weed plants were selected and marked (Figure 3). To locate individual weeds in the orthophoto manually, the Create Feature Class tool in the geoprocessing tool kit of ArcGIS Pro software was used. The *Point Feature* function was selected to mark *P. annua* in the orthophoto, and the resulting feature class was exported to a CSV file. Subsequently, the same orthophoto was used for weed detection and localization using a custom-trained weed model. Both model output formats, CSV and shapefile, were exported for accuracy assessment. The resulting shapefile was then superimposed on the orthophoto to visualize the weed locations identified by the model. To quantify the difference between the manually marked weed positions and the model-predicted positions, distances were calculated using the *geodesic*

Downloaded from https://www.cambridge.org/core. UNIVERSIDAD AUTONOMA METROPOLITANA, on 16 Nov 2026 at 20:06:17, subject to the Cambridge Core terms of use, available at https://www.cambridge.org/core/terms. https://doi.org/10.1017/wsc.2026.10104



**Figure 3.** An example image showing the manual marking of *Poa annua* in bermudagrass turf to verify the accuracy of weed localization. For the final comparison, only individual weeds without occlusion were selected to avoid manual errors when locating overlapping weed centroids.

function in the geopy package (Anonymous 2018; Equation 3). Root mean-square error (RMSE), mean, and SE were also calculated.

$$\text{Distance} = \text{geopy.distance.geodesic}(\text{coords_1}, \text{coords_2}).\text{m} \quad [3]$$

where coords_1 denotes the manually located weed centroid, and coords_2 represents the model-predicted weed centroid.

### Path Planning for SSWC

Two heuristic algorithms, nearest neighbor (NN) and ant colony optimization (ACO), were used to determine the shortest navigation path length for SSWC. The NN algorithm is deterministic, starting at an initial point (i.e., fixed) and iteratively moving to the nearest unvisited location until all spots are covered. In contrast, ACO is a probabilistic algorithm inspired by the behavior of ants searching for food, in which they deposit pheromones along their paths and tend to follow routes with stronger pheromone levels. To optimize the path for spot spraying, two separate Python scripts were written to implement these algorithms. For the ACO algorithm, the following parameters were chosen: num_ants = 200, num_iterations = 100, alpha = 1, beta = 2, and evaporation rate = 0.5 (https://github.com/Akavall/AntColonyOptimization). To evaluate the algorithms, 10 random images were selected, and weed coordinates were extracted using the custom-trained weed detection model. The algorithms were then used to arrange the extracted coordinates in the shortest path. The Haversine formula was applied to calculate the cumulative distance ($D$) (Anonymous n.d.; Equation 4).

$$D = \text{haversine}(\theta) = \sin^2(\theta/2) \quad [4]$$

where θ is the central angle between two points on the surface of a sphere, typically measured in radians. To compare the effectiveness of the PPAs, a one-way ANOVA was performed using the statistical software JMP® Pro v. 16.0. Before ANOVA, the cumulative distance data were log transformed in Microsoft Excel 2019 (Microsoft, Seattle, WA, USA).

## Results and Discussion

### Poa annua Detection and Model Comparison

A comprehensive evaluation of the YOLO11 and transformer (RT-DETR) models demonstrated consistent performance in detecting *P. annua* on a bermudagrass background (Table 1). However, in terms of inference speed, the YOLO11n variant outperformed all other variants without compromising model performance (Figures 4 and 5). Among the YOLO11 variants, YOLO11n demonstrated the best performance, achieving an F1 score of 0.646 and a mAP@0.50 of 0.682, yet it was comparable to the other variants tested (Table 1). This includes the RT-DETR model variants RT-DETR-l and RT-DETR-x.

The models evaluated in this study demonstrate excellent performance compared with results from several previous studies on weed detection in actively growing turf. For instance, Zhuang et al. (2022) found F1-score values of only 0.56 for YOLOv3, 0.53 for Faster R-CNN, and 0.53 for VFNet for general weed detection in bahiagrass (*Paspalum notatum* Flueggé). In another study, Yu et al. (2019a) reported F1 scores of 0.99, 0.66, and 0.94 for DetectNet, GoogLeNet, and VGGNet, respectively, in detecting *P. annua* within dormant bermudagrass. The dataset used by Yu et al. (2019a) was small, featured a simple turf background (i.e., green on brown), and consisted of proximal images. In comparison, the models presented in this study exhibit stronger generalization capability, as they were trained on a robust UAS imagery dataset. The dataset included complex backgrounds (grass [*P. annua*] within grass [bermudagrass]), sparse weed distribution, varying growth stages, diverse turf environments, and varying mowing conditions (Figures 1 and 6).

The model metrics from this research are still low, indicating room for improvement. The low spatial resolution of UAS imagery, the UAS's broader field of view, large-scale variations in *P. annua* instances, and the background complexity likely contributed to the lower metric scores (Gurjar et al. 2025). Additionally, detecting *P. annua* at early growth stages and in freshly mown fields was challenging in autonomous flight mode images (Figure 7). These results are consistent with those of Zhang et al. (2021), who reported reduced CNN model performance for weed detection in sod production fields using UAS imagery, attributing it to its lower spatial resolution. However, spatial resolution and *P. annua* detection at the early growth stage may be improved by splitting the images into sub-images according to the model's preferred input size (Figure 8). This method allows for the preservation of spatial resolution during model training, thus mitigating computational resource consumption (Jiang et al. 2022). Nevertheless, the primary objective was to employ original UAS-collected images for weed detection within turf systems, which led us to refrain from adopting the image-splitting approach.

### Weed Localization Accuracy Assessment

Positional error reflects the variance in estimating the center point of a weed between the model-predicted centroid and the manually marked centroid. This error is influenced by the geometry of the

Downloaded from https://www.cambridge.org/core. UNIVERSIDAD AUTONOMA METROPOLITANA, on 16 Nov 2026 at 20:06:17, subject to the Cambridge Core terms of use, available at https://www.cambridge.org/core/terms. https://doi.org/10.1017/wsc.2026.10104

**Table 1.** Performance metrics (F1 score, precision, recall, and mAP@0.50) obtained during the evaluation of YOLO11 and RT-DETR model variants for *Poa annua* recognition in bermudagrass.

| Model variants | Precision[a] | Recall | F1 Score | mAP@0.50 |
|---|---|---|---|---|
| YOLO11n | 0.626 ± 0.009 a | 0.668 ± 0.011 a | 0.646 ± 0.010 a | 0.682 ± 0.015 a |
| YOLO11s | 0.627 ± 0.009 a | 0.654 ± 0.009 a | 0.640 ± 0.009 a | 0.677 ± 0.015 a |
| YOLO11m | 0.613 ± 0.010 a | 0.658 ± 0.012 a | 0.634 ± 0.010 a | 0.669 ± 0.014 a |
| YOLO11l | 0.602 ± 0.008 a | 0.645 ± 0.011 a | 0.622 ± 0.009 a | 0.651 ± 0.014 a |
| YOLO11x | 0.619 ± 0.013 a | 0.651 ± 0.010 a | 0.634 ± 0.011 a | 0.657 ± 0.014 a |
| RT-DETR-l | 0.605 ± 0.008 a | 0.637 ± 0.012 a | 0.620 ± 0.010 a | 0.645 ± 0.013 a |
| RT-DETR-x | 0.500 ± 0.098 a | 0.554 ± 0.069 a | 0.522 ± 0.088 a | 0.517 ± 0.104 a |

[a]Means ± SE within a column followed by a common letter are not significantly different based on Tukey's honestly significant difference (HSD) test (α = 0.05).

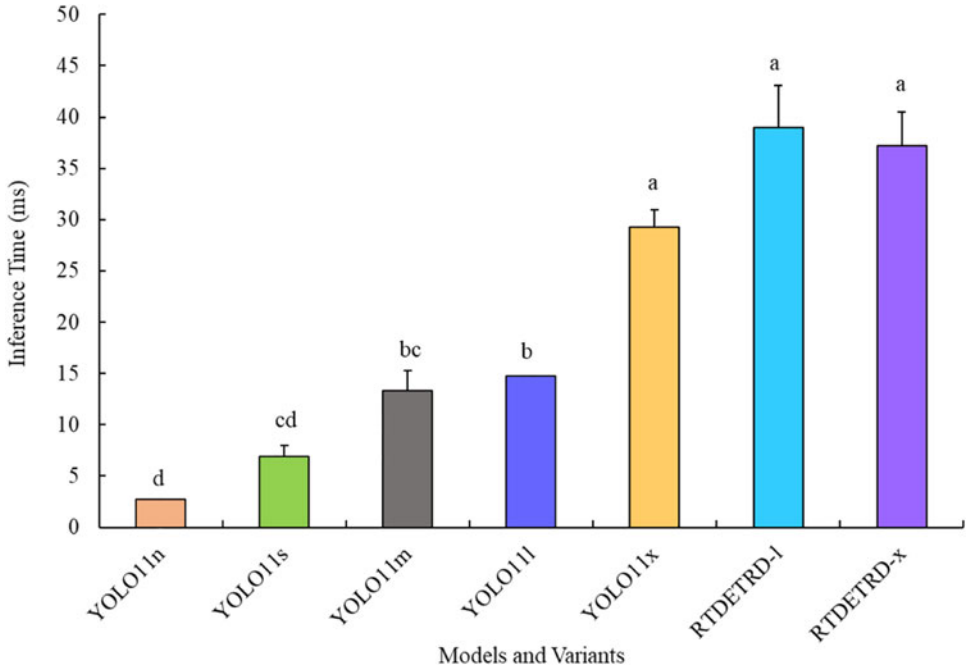



**Figure 4.** Inference time (in milliseconds) incurred per image during the validation of YOLO11 and RT-DETR model variants on 31,000 instances of *Poa annua*, using Ubuntu 20.04.4 LTS with an NVIDIA RTX A6000 graphics processing unit (50-GB memory) and 250-GB RAM. The whiskers represent the standard errors of the mean. Bars topped by different letters indicate significant differences based on Tukey's honestly significant difference (HSD) test (α = 0.05).

individual weed and the accuracy of orthophoto georeferencing (Gurjar et al. 2026; Oh et al. 2020). For manual marking, the visually estimated center location for individual weeds was successfully pinpointed. The model-predicted weed centroid, on the other hand, was determined based on the center point of the bounding box; thus, the accuracy depends on how tightly the weed fits within the bounding box (Figure 9). The findings indicate that the RMSE between the manually marked and model-predicted coordinates was 0.4 cm ($n = 119$). The mean, standard deviation, and SE were 1.5 cm, 1.2 cm, and 0.1 cm, respectively (Figure 10). These results show that model-predicted coordinates have centimeter-level accuracy, which is operationally precise for herbicide treatments. In a similar study by Zhang et al. (2020) focusing on weed localization in a wheat (*Triticum aestivum* L.) crop, the positional error ranged from 0 to 20 cm; the misalignment of pixel positions on the image plane during the transformation from image pixel coordinates to world coordinates likely caused these errors. Additionally, weed localization accuracy can be affected by the orthomosaic georeferencing accuracy. The RMSE of orthophotos was observed in the longitude and latitude directions of 0.823 cm and 0.678 cm, respectively. In this regard, Benassi et al. (2017) reported an RMSE of 2 to 3 cm for the orthomosaic image using eBEE-RTK.

## Optimization of Path Length for Spot Spraying

The NN and ACO algorithms provided a significant reduction in path length for spot spraying, reducing the path length by 37.7% and 36.7%, respectively, compared with the original distance ($P = 0.0053$) (Figure 11). Although the NN algorithm performed better than the ACO algorithm, the difference between them was not statistically significant ($P = 0.999$). These reductions in path length significantly enhance the effectiveness of UAS and robots, allowing them to autonomously execute tasks in a highly efficient manner (Alamgir and Von Luxburg 2012). Additionally, the improved path efficiency translates to better battery performance, enabling UAS and robots to cover larger areas with the same battery capacity (Figure 12). The NN algorithm prioritizes the

Downloaded from https://www.cambridge.org/core. UNIVERSIDAD AUTONOMA METROPOLITANA, on 16 Nov 2026 at 20:06:17, subject to the Cambridge Core terms of use, available at https://www.cambridge.org/core/terms. https://doi.org/10.1017/wsc.2026.10104




**Figure 5.** Example of *Poa annua* detection using an unmanned aerial system (UAS) in autonomous flight mode using the YOLO11n model. The autonomous flight was conducted at 5-m altitude when the bermudagrass was actively growing. (A) An original raw UAS imagery and (B) the raw image transformed into a georeferenced image using a photogrammetry software (Agisoft Metashape).

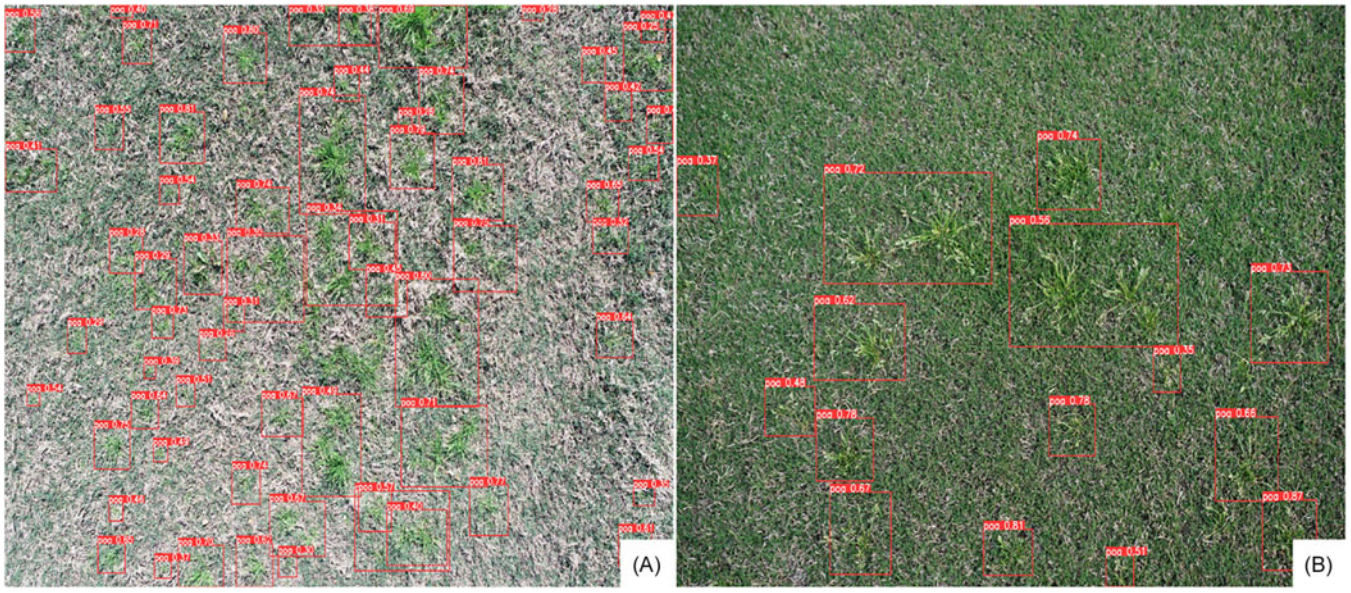



**Figure 6.** Example of *Poa annua* detection in bermudagrass turf using unmanned aerial system (UAS) imagery and YOLO11n model: (A) detection in dormant bermudagrass at an early weed growth stage and (B) detection in actively growing bermudagrass at the flowering stage. These images were collected in manual flight mode at an altitude of approximately 3 m.

shortest distance to the next available neighboring points; it may not always yield the most optimal route from the starting point to the endpoint, but it yields a shorter route. Moreover, the NN algorithm does not always mimic human intuition in finding optimal paths (Wiener et al. 2007), but it exhibits promise in finding the shortest path length.

This study represents a pioneering effort to explore the use of UAS imagery for detecting and localizing *P. annua* within bermudagrass turf systems. Despite a complex dataset with variable growth stages of *P. annua* and varying turfgrass conditions, the results demonstrate the potential of utilizing UAS imagery and ML models for weed detection in these systems. However, the weed recognition model exhibited suboptimal performance due to the intricate nature of the dataset, characterized by instances of spectral/textural similarity, as well as limitations in the model's architecture, such as the need to downscale UAS images during model training. This downscaling likely led to the omission of small *P. annua* plants due to lower spatial resolution. Even with

Downloaded from https://www.cambridge.org/core. UNIVERSIDAD AUTONOMA METROPOLITANA, on 16 Nov 2026 at 20:06:17, subject to the Cambridge Core terms of use, available at https://www.cambridge.org/core/terms. https://doi.org/10.1017/wsc.2026.10104

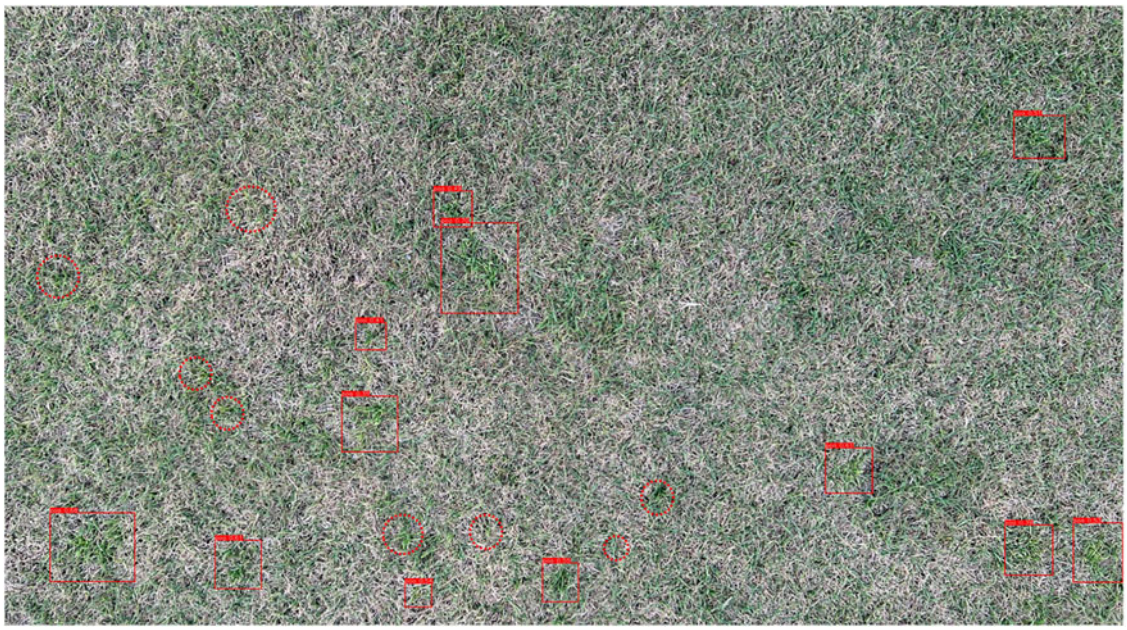


**Figure 7.** Detection of *Poa annua* using YOLOv11n in a freshly mowed field (mowing height = 1.25 cm). Rectangular boxes indicate weeds correctly detected by the model, whereas circles denote weeds that were missed. This example illustrates the model's limitations under freshly mowed conditions, where *P. annua* plants are partially camouflaged by the surrounding bermudagrass.

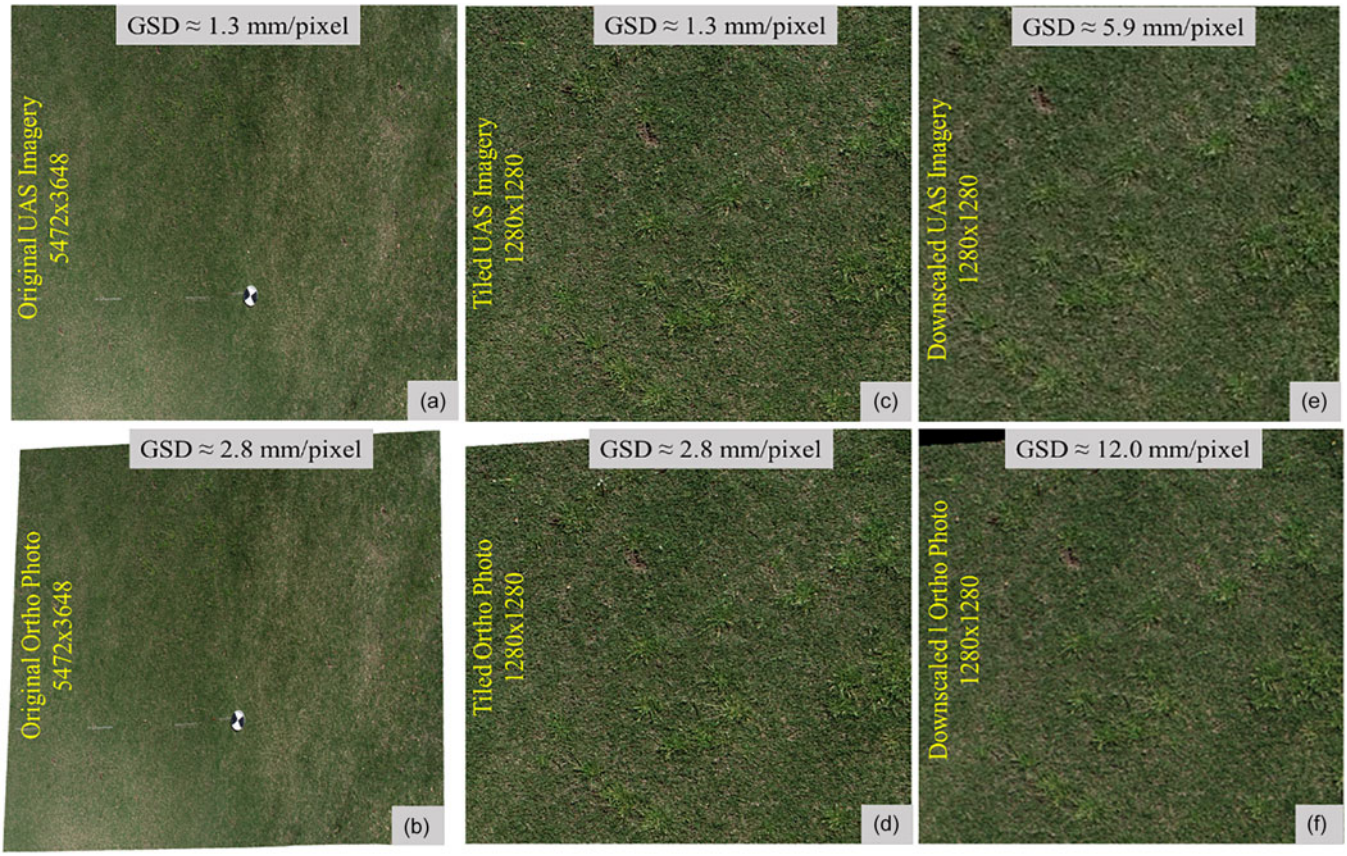



**Figure 8.** Example illustrating how decreasing spatial resolution reduces object detail: (A) Original unmanned aerial system (UAS) imagery; (B) original orthomosaic imagery; (C) image from A divided into 1,280 × 1,280 pixel tiles; (D) image from B divided into 1,280 × 1,280 pixel tiles; (E) the UAS imagery downscaled to 1,280 × 1,280 pixels; (F) the orthomosaic imagery downscaled to 1,280 × 1,280 pixels.

Downloaded from https://www.cambridge.org/core. UNIVERSIDAD AUTONOMA METROPOLITANA, on 16 Nov 2026 at 20:06:17, subject to the Cambridge Core terms of use, available at https://www.cambridge.org/core/terms. https://doi.org/10.1017/wsc.2026.10104

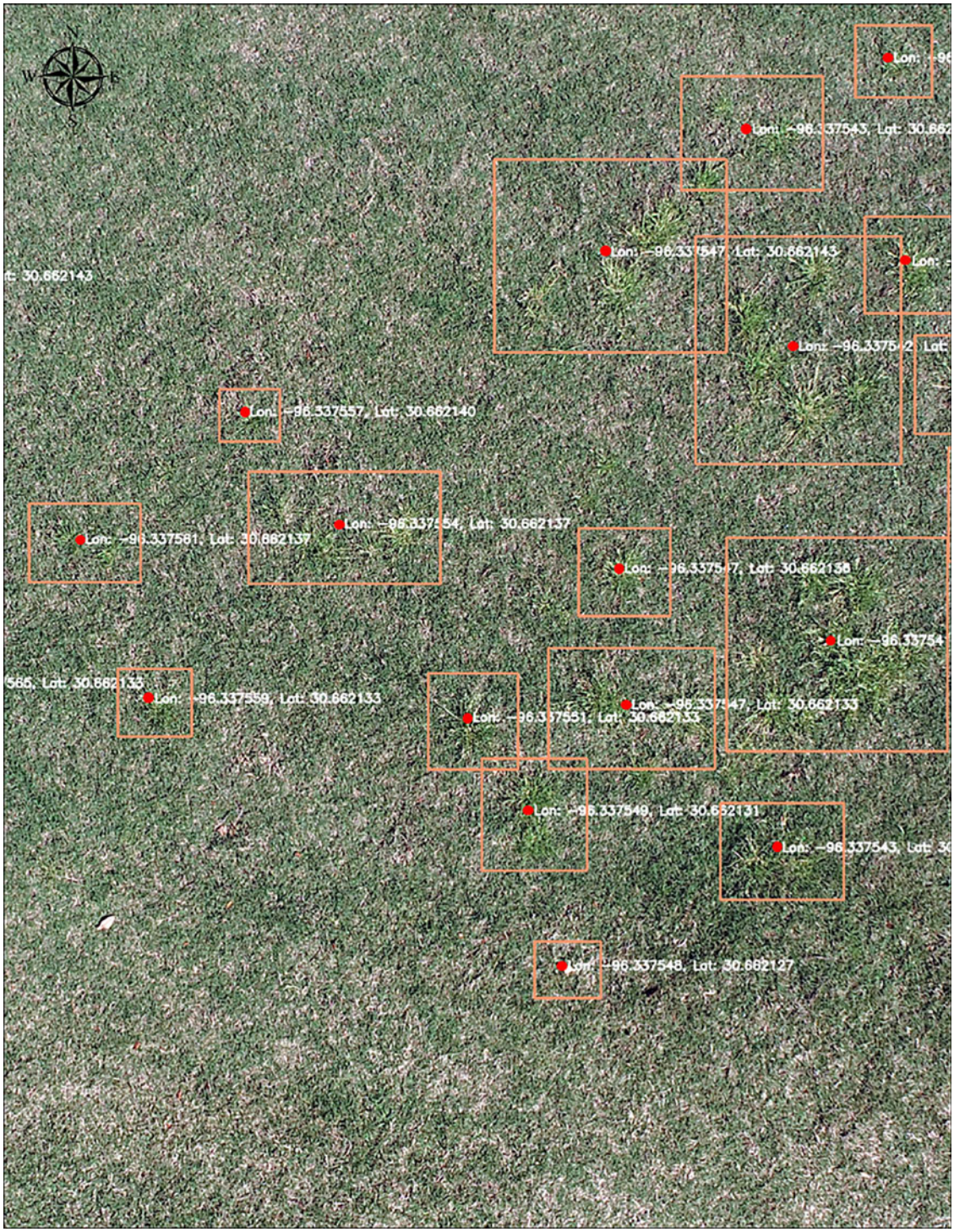



**Figure 9.** Example of the accuracy of model-predicted *Poa annua* weed centroids, showing how tightly the weed(s) fit within the bounding box. The YOLO11n model was used to detect weeds in an orthophoto, with the original image captured using an unmanned aerial system at 5-m altitude in the autonomous flight mode.

different model architectures (e.g., YOLO and RT-DETR), the models struggled to detect smaller weeds effectively. If UAS imagery is to be employed for weed detection in turfgrass systems, our findings strongly advocate either modifying the model architecture or splitting the original images into sub-images to preserve the spatial resolution of UAS imagery. Additionally, the GeoTransform function effectively transformed image coordinates into a world coordinate system with centimeter-level accuracy (mean = 1.5 cm); however, transformation accuracy depends on the accuracy of the orthophoto georeferencing. Moreover, the NN PPA arranges the weed coordinates based on the shortest distance from the nearest neighbor's point, enabling

Downloaded from https://www.cambridge.org/core. UNIVERSIDAD AUTONOMA METROPOLITANA, on 16 Nov 2026 at 20:06:17, subject to the Cambridge Core terms of use, available at https://www.cambridge.org/core/terms. https://doi.org/10.1017/wsc.2026.10104



**Figure 10.** Examples of displacement of the custom trained model-predicted *Poa annua* weed centroid (plus sign) from the manually marked weed center point (star sign). To visualize the difference between them, these weed centroids are overlaid on the orthophoto.

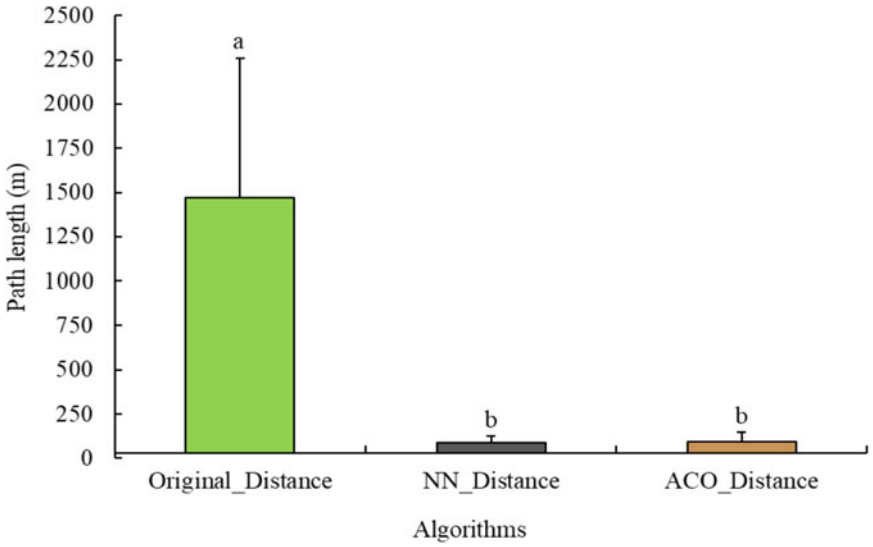



**Figure 11.** Path length compression among the three algorithms used: original coordinates, nearest neighbor (NN) algorithm, and ant colony optimization (ACO) algorithm. The whiskers represent the standard errors of the mean. Bars topped by different letters indicate significant differences based on Tukey's honestly significant difference (HSD) test ($\alpha = 0.05$).

Downloaded from https://www.cambridge.org/core. UNIVERSIDAD AUTONOMA METROPOLITANA, on 16 Nov 2026 at 20:06:17, subject to the Cambridge Core terms of use, available at https://www.cambridge.org/core/terms. https://doi.org/10.1017/wsc.2026.10104

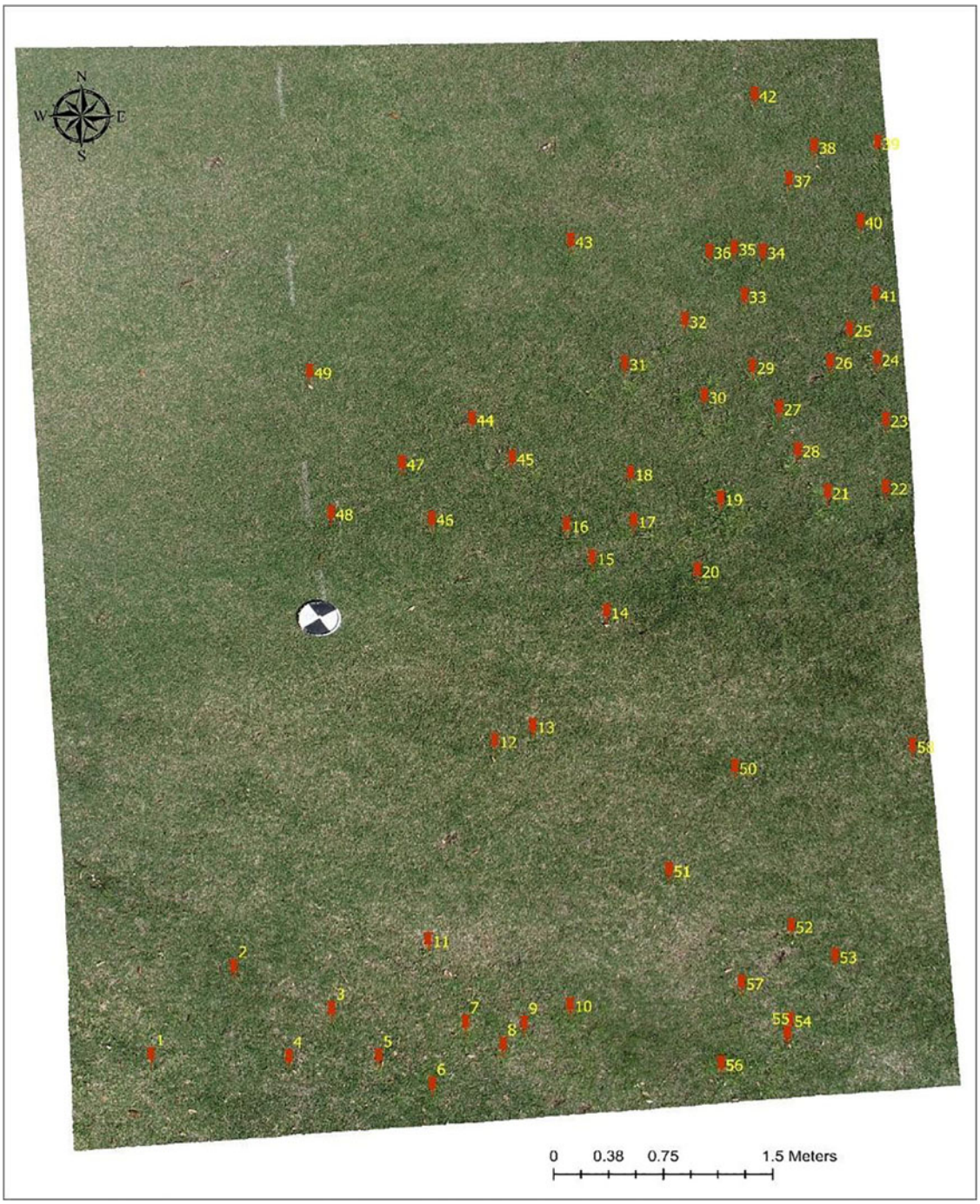



**Figure 12.** Example of a path planning algorithm (PPA) (nearest neighbor [NN]) arranging weed coordinates based on the shortest distance to unvisited weeds. To visualize the coordinate arrangement, an orthophoto was used, with the coordinates overlaid on it.

operators to autonomously execute tasks in a highly time-efficient manner. The developed model has the potential to be used for site-specific herbicide applications in turf to manage individual *P. annua* plants using UAS, ground robots, or global navigation satellite system-guided boom sprayers. However, future efforts should focus on enhancing model performance by altering the model architecture and evaluating its robustness across different weed growth stages and various turf species backgrounds. Future research should also focus on developing methods for weed detection in turf when multiple weeds occur together and create occlusion.

**Data availability.** The dataset and model will be available publicly through the International Weed Recognition Consortium Website (https://www.weedrecognition.org/) upon publication.

**Acknowledgments.** BG acknowledges a graduate fellowship from the Nethaji-Subhash International Fellowship Program of the Indian Government.

**Funding.** This work was funded in part by PBI-Gordon Corporation.

**Competing interests.** The authors declare that no competing interests exist.

Downloaded from https://www.cambridge.org/core. UNIVERSIDAD AUTONOMA METROPOLITANA, on 16 Nov 2026 at 20:06:17, subject to the Cambridge Core terms of use, available at https://www.cambridge.org/core/terms. https://doi.org/10.1017/wsc.2026.10104

## References


Alamgir M, Von Luxburg U (2012) Shortest path distance in random k-nearest neighbor graphs. arXiv preprint arXiv:1206.6381

Anonymous (2018) Geopy package. https://geopy.readthedocs.io/en/stable/#module-geopy.distance. Accessed: August 13, 2025

Anonymous (2025) GDAL package. https://gdal.org/tutorials/geotransforms_tut.html. Accessed: August 9, 2025

Anonymous (n.d.) Distance between Points on the Earth's Surface. https://www.math.ksu.edu/~dbski/writings/haversine.pdf. Accessed: January 13, 2026

Balogh JC, Anderson JL (2020) Environmental impacts of turfgrass pesticides. Pages 221–353 *in* Golf Course Management & Construction: Environmental Issues. Boca Raton, FL: CRC Press. https://doi.org/10.1201/9781003070092

Beckie HJ (2006) Herbicide-resistant weeds: management tactics and practices. Weed Technol 20:793–814

Benassi F, Dall'Asta E, Diotri F, Forlani G, Morra di Cella U, Roncella R, Santise M (2017) Testing accuracy and repeatability of UAV blocks oriented with GNSS-supported aerial triangulation. Remote Sens 9:172

Breeden SM, Brosnan JT, Mueller TC, Breeden GK, Horvath BJ, Senseman SA (2017) Confirmation and control of annual bluegrass (*Poa annua*) with resistance to prodiamine and glyphosate. Weed Technol 31:111–119

Brosnan JT, Breeden GK, Zobel JM, Patton AJ, Law QD (2020a) Nonchemical annual bluegrass (*Poa annua*) management in zoysiagrass via fraise mowing. Weed Technol 34:482–488

Brosnan JT, Elmore MT, Bagavathiannan MV (2020b) Herbicide-resistant weeds in turfgrass: current status and emerging threats. Weed Technol 34:424–430

Busey P (2003) Cultural management of weeds in turfgrass: a review. Crop Sci 43:1899–1911

Coleman GR, Bender A, Hu K, Sharpe SM, Schumann AW, Wang Z, Bagavathiannan MV, Boyd NS, Walsh MJ (2022) Weed detection to weed recognition: reviewing 50 years of research to identify constraints and opportunities for large-scale cropping systems. Weed Technol 36:741–757

DeBels BT, Griffith SE, Kreuser WC, Melby ES, Soldat, DJ (2012) Evaluation of mowing height and fertilizer application rate on quality and weed abundance of five home lawn grasses. Weed Technol 26:826–831

Esposito M, Crimaldi M, Cirillo V, Sarghini F, Maggio A (2021) Drone and sensor technology for sustainable weed management: a review. Chem Bio Technol Agric 8:1–11

Gerhards R, Oebel H (2006) Practical experiences with a system for site-specific weed control in arable crops using real-time image analysis and GPS-controlled patch spraying. Weed Res 46:185–193

Gurjar B, Sapkota B, Torres U, Ceperkovic I, Kutugata M, Kumar V, Zhou XG, Martin D, Bagavathiannan M (2025) Site-specific treatment of late-season weed escapes in rice utilizing a remotely piloted aerial application system. Weed Technol 39:e74

Gurjar B, Torres, U, Coleman, G, Straw, CM, Bagavathiannan M (2026) Effect of mowing, imaging technique, and annotation method on weed detection in turfgrass using Yolo. Precis Agric 27:46

Hahn DS, Roosjen P, Morales A, Nijp J, Beck L, Velasco Cruz C, Leinauer B (2021) Detection and quantification of broadleaf weeds in turfgrass using close-range multispectral imagery with pixel-and object-based classification. Int J Remote Sens 42:8035–8055

Jiang P, Ergu D, Liu F, Cai Y, Ma B (2022) A review of Yolo algorithm developments. Procedia Comput Sci 199:1066–1073

Jin X, Bagavathiannan M, McCullough PE, Chen Y, Yu J (2022) A deep learning-based method for classification, detection, and localization of weeds in turfgrass. Pest Manag Sci 78:4809–4821

Jin X, McCullough PE, Liu T, Yang D, Zhu W, Chen Y, Yu J (2023) A smart sprayer for weed control in bermudagrass turf based on the herbicide weed control spectrum. Crop Prot 170:106270

McCurdy JD, Bowling RG, de Castro EB, Patton AJ, Kowalewski AR, Mattox CM, Brosnan JT, Ervin DE, Askew SD, Goncalves CG (2023) Developing and implementing a sustainable, integrated weed management program for herbicide-resistant *Poa annua* in turfgrass. Crop Forage Turfgrass Manag 9:e20225

Neal JC (2024) Biological control of weeds in turfgrass: opportunities and misconceptions. Pest Manag Sci 80:40–48

Oh S, Chang A, Ashapure A, Jung J, Dube N, Maeda M, Gonzalez D, Landivar J (2020) Plant counting of cotton from UAS imagery using deep learning-based object detection framework. Remote Sens 12:2981

Parra L, Marin J, Yousfi S, Rincón G, Mauri PV, Lloret J (2020) Edge detection for weed recognition in lawns. Comput Electron Agric 176:105684

Patton AJ, Braun RC, Schortgen GP, Weisenberger DV, Branham BE, Sharp B, Sousek MD, Gaussoin RE, Reicher ZJ (2019) Long-term efficacy of annual bluegrass control strategies on golf course putting greens. Crop Forage Turfgrass Manag 5:1–10

Petelewicz P, Zhou Q, Schiavon M, MacDonald GE, Schumann AW, Boyd NS (2024) Simulation-based nozzle density optimization for maximized efficacy of a machine vision–based weed control system for applications in turfgrass settings. Weed Technol 38:e25

Plessen M (2025) Path planning for spot spraying with UAVs combining TSP and area coverages. Smart Agric Technol 11:100965

Rai N, Zhang Y, Ram BG, Schumacher L, Yellavajjala RK, Bajwa S, Sun X (2023) Applications of deep learning in precision weed management: a review. Comput Electron Agric 206:107698

Scherner A, Melander B, Jensen PK, Kudsk P, Avila LA (2017) Germination of winter annual grass weeds under a range of temperatures and water potentials. Weed Sci 65:468–478

Swinton SM (2005) Economics of site-specific weed management. Weed Sci 53:259–263

Tu M, Hurd C, Randall JM (2001) Weed Control Methods Handbook: Tools & Techniques for Use in Natural Areas. The Nature Conservancy. https://tncweeds.ucdavis.edu

Tzutalin D (2015) LabelImg. GitHub repository. https://github.com/byhqsr/tzutalin-labelImg. Accessed: May 12, 2025

Vijayakumar S, Gurjar B, Bagavathiannan M, Kumar V (2025) The role of unmanned aerial vehicles and sensor technology in site-specific weed management. Pages 89–123 *in* Chauhan BS, Mahajan G, eds. Recent Advances in Weed Science. Cham: Springer Nature Switzerland.

Westwood JH, Charudattan R, Duke SO, Fennimore SA, Marrone P, Slaughter DC, Swanton C, Zollinger R (2018) Weed management in 2050: perspectives on the future of weed science. Weed Sci 66:275–285

Wiener JM, Ehbauer NN, Mallot HA (2007) Path planning and optimization in the traveling salesman problem: nearest neighbor vs. region-based strategies. Pages 1–21 *in* Dagstuhl Seminar Proceedings 5491. Schloss-Dagstuhl-Leibniz Zentrum für Informatik. https://doi.org/10.4230/DagSemProc.05491.7

Wong TT, Yeh PY (2019) Reliable accuracy estimates from k-fold cross validation. IEEE Transac Knowledge Data Eng 32:1586–1594

Xie S, Hu C, Bagavathiannan M, Song D (2021) Toward robotic weed control: detection of nutsedge weed in bermudagrass turf using inaccurate and insufficient training data. IEEE Robot Autom Lett 6:7365–7372

Yacouby R, Axman D (2020) Probabilistic extension of precision, recall, and f1 score for more thorough evaluation of classification models. Pages 79–91 *in* Proceedings of the First Workshop on Evaluation and Comparison of NLP systems. Association for Computational Linguistics

Yu J, Schumann AW, Cao Z, Sharpe SM, Boyd NS (2019a) Weed detection in perennial ryegrass with deep learning convolutional neural network. Front Plant Sci 10:1422

Yu J, Sharpe SM, Schumann AW, Boyd NS (2019b) Deep learning for image-based weed detection in turfgrass. Eur J Agron 104:78–84

Zhang J, Maleski J, Jespersen D, Waltz F Jr, Rains G, Schwartz B (2021) Unmanned aerial system-based weed mapping in sod production using a convolutional neural network. Front Plant Sci 12:702626

Zhang R, Wang C, Hu X, Liu Y, Chen S (2020) Weed location and recognition based on UAV imaging and deep learning. Int J Precis Agric Aviat 3:23–29

Zhao Y, Lv W, Xu S, Wei J, Wang G, Dang Q, Liu Y, Chen J (2024) DETRs beat YOLOs on real-time object detection. Pages 16965–16974 *in* Proceedings of the IEEE/CVF Conference on Computer Vision and Pattern Recognition (CVPR), Seattle, WA, USA. 16–22 June 2024. https://doi.org/10.1109/CVPR52733.2024.01605

Zhuang J, Jin X, Chen Y, Meng W, Wang Y, Yu J, Muthukumar B (2022) Drought stress impact on the performance of deep convolutional neural networks for weed detection in Bahiagrass. Grass Forage Sci 78:214–223


Downloaded from https://www.cambridge.org/core. UNIVERSIDAD AUTONOMA METROPOLITANA, on 16 Nov 2026 at 20:06:17, subject to the Cambridge Core terms of use, available at https://www.cambridge.org/core/terms. https://doi.org/10.1017/wsc.2026.10104